

REFERENCES AND NOTES

1. A. Banerjee *et al.*, *Science* **263**, 227 (1994); A. Des- sen, A. Quémard, J. S. Blanchard, W. R. Jacobs Jr., J. C. Sacchettini, *ibid.* **267**, 1638 (1995).
2. H. Bergler *et al.*, *J. Biol. Chem.* **269**, 5493 (1994).
3. S. T. Cole, *Trends Microbiol.* **2**, 411 (1994).
4. G. Högenauer and M. Woisetschlager, *Nature* **293**, 662 (1981).
5. M. M. Kater, G. M. Koningstein, H. J. J. Nijkamp, A. R. Stuitje, *Plant Mol. Biol.* **25**, 771 (1994).
6. *Escherichia coli* ENR is a homotetramer ($M_r \sim 28,000$ per subunit) that was prepared from an overexpressing *E. coli* strain (2, 5). Crystals of the ENR-NAD⁺ complex (crystal form A) belong to space group $P2_1$ and have unit cell dimensions of $a = 74.0 \text{ \AA}$, $b = 81.2 \text{ \AA}$, $c = 79.0 \text{ \AA}$, and $\beta = 92.9^\circ$ with a tetramer in the asymmetric unit (16). Data were collected to 2.5 \AA (Table 1, data set Native-1) on a twin San Diego Multiwire Systems (SDMS) area detector with a Rigaku RU-200 rotating anode source, and the data set was processed with SDMS software (17). Data were also collected to 2.1 \AA (Table 1, data set Native-2) at the CLRC Daresbury Synchrotron and processed with the MOSFLM package (18), and the 2.1 and 2.5 \AA data sets were then scaled and merged with CCP4 software (19). Initially, a model of *B. napus* ENR (10) was used as a basis for a molecular replacement solution of the structure, but the map, calculated after the model was refined with the program TNT (20), was not of sufficient quality to confidently assign residues in regions of structural differences between the *B. napus* and *E. coli* enzymes. Therefore, to solve the structure, we obtained a heavy-atom derivative by soaking an ENR-NAD⁺ (form A) crystal for 1 hour in 0.1 M ethylenediaminetetraacetate, 10 mM NAD⁺, 20% (w/v) polyethylene glycol (molecular weight 400), and 100 mM acetate (pH 5.0). Derivative data were collected at the CLRC Daresbury Synchrotron to a resolution of 3 \AA (Table 1, data set Hg) and were processed as above. The positions of the heavy atoms in this derivative were revealed by difference Fourier methods with the use of the approximate phases provided by the molecular replacement solution. The heavy-atom parameters were refined with the program MLPHARE (21) and resulted in a phase set with an overall mean figure of merit of 0.34 to 3 \AA resolution. Using a map derived from these phases, we generated molecular masks for the molecule with the program MAMA (22) and performed 50 cycles of solvent flattening and fourfold molecular averaging with the program DM (19, 23). In the resultant electron density map, calculated from the averaged phases, we were able to find clear density for all but the first residue, the last four residues, and 10 residues from the loop joining $\beta 6$ and $\alpha 6$; using the graphics program FRODO (24), we were able to build with confidence a model comprising 247 of the 262 amino acids of *E. coli* ENR. Several cycles of rebuilding and refinement gave a final R factor for the model of 0.157 ($52,346$ reflections in the range 10 to 2.1 \AA , 7836 atoms including 324 water molecules), with an rmsd of 0.017 \AA for bonds and 2.92° for angles [$R = \frac{\sum (|F_{\text{obs}}| - |F_{\text{calc}}|)}{\sum (|F_{\text{obs}}|)}$, where $|F_{\text{obs}}|$ and $|F_{\text{calc}}|$ are the observed and calculated structure factor amplitudes, respectively]. The average B factor for the tetramer is 30 \AA^2 (24 \AA^2 for main-chain atoms), where $B = 8\pi^2 \langle \delta^2 \rangle$ and δ is the mean square displacement of the atomic vibration.
7. Crystals of the ENR-NAD⁺-diazaborine complex (crystal form B) belong to space group $P6_122$ and have unit cell dimensions of $a = b = 80.9 \text{ \AA}$, $c = 328.3 \text{ \AA}$, $\alpha = \beta = 90^\circ$, and $\gamma = 120^\circ$ for the thienodiazaborine complex, and $a = b = 80.6 \text{ \AA}$, $c = 325.3 \text{ \AA}$, $\alpha = \beta = 90^\circ$, and $\gamma = 120^\circ$ for the benzodiazaborine complex with a dimer in the asymmetric unit (16). Data sets were collected on the ENR-NAD⁺-thienodiazaborine complex to 2.2 \AA and on the ENR-NAD⁺-benzodiazaborine complex to 2.5 \AA (Table 1, data sets Thieno and Benzo) at the CLRC Daresbury Synchrotron and were processed as above. The structures of both ENR-NAD⁺-diazaborine complexes were solved independently by molecular replacement with the use of an appropriate dimer from the *E. coli* ENR-NAD⁺ structure and were refined against their respective data sets with the program TNT (20). The initial electron density maps were readily interpretable and unambiguous density could be observed for the location of the diazaborine compounds, which were then incorporated into the refinement. Clear density could be found for all but the first residue and the last four residues. Refinement of the thienodiazaborine complex gave a final R factor of 0.191 ($30,825$ reflections in the range 10 to 2.2 \AA , 3936 atoms), with an rmsd of 0.012 \AA for bonds and 2.9° for angles. The average B factor for the dimer is 27 \AA^2 (22 \AA^2 for main-chain atoms, 20 \AA^2 for diazaborine atoms). Refinement of the benzodiazaborine complex gave a final R factor of 0.169 ($20,204$ reflections in the range 10 to 2.5 \AA , 3930 atoms), with an rmsd of 0.013 \AA for bonds and 2.7° for angles. The average B factor for the dimer is 24 \AA^2 (20 \AA^2 for main-chain atoms, 20 \AA^2 for diazaborine atoms). For the ENR-NAD⁺ complex and the ENR-NAD⁺-thienodiazaborine complex, $244 \text{ C}\alpha$ atoms superimpose with an rmsd of 0.3 \AA , whereas for the two ENR-NAD⁺-diazaborine complexes, $256 \text{ C}\alpha$ atoms superimpose with an rmsd of 0.2 \AA .
8. M. A. Grassberger, F. Turnowsky, J. Hildebrandt, *J. Med. Chem.* **27**, 947 (1984).
9. S. Zhong, F. Jordan, C. Kettner, L. Polgar, *J. Am. Chem. Soc.* **113**, 9429 (1991).
10. J. B. Rafferty *et al.*, *Structure* **3**, 927 (1995).
11. H. Bergler, G. Högenauer, F. Turnowsky, *J. Gen. Microbiol.* **138**, 2093 (1992).
12. C. Taillefumier, D. de Fornel, Y. Chapleur, *Bioorg. Med. Chem. Lett.* **6**, 615 (1996).
13. J. T. Bolin, D. J. Filman, D. A. Matthews, R. C. Hamlin, J. Kraut, *J. Biol. Chem.* **257**, 13650 (1982); C. Byströf, S. J. Oatley, J. Kraut, *Biochemistry* **29**, 3263 (1990).
14. H. G. Bull *et al.*, *J. Am. Chem. Soc.* **118**, 2359 (1996).
15. M. D. Sintchak *et al.*, *Cell* **85**, 921 (1996).
16. C. Baldock *et al.*, *Acta Crystallogr.*, in press.
17. R. Hamlin, *Methods Enzymol.* **114**, 416 (1985); A. J. Howard, C. Nielson, N. H. Xuong, *ibid.*, p. 452; N. H. Xuong, C. Nielson, R. Hamlin, D. Anderson, *J. Appl. Crystallogr.* **18**, 342 (1985).
18. A. G. W. Leslie, *Joint CCP4 and ESF-EACBM Newsletter on Protein Crystallography No. 26* (SERC Daresbury Laboratory, Warrington, UK, 1992).
19. Collaborative Computational Project No. 4, *Acta Crystallogr.* **D50**, 760 (1994).
20. D. E. Tronrud, L. F. Ten Eyck, B. W. Matthews, *ibid.* **A43**, 489 (1987).
21. Z. Otwinowski, in *Proceedings of the CCP4 Study Weekend*, W. Wolf, P. R. Evans, A. G. W. Leslie, Eds. (SERC Daresbury Laboratory, Warrington, UK, 1991), p. 80.
22. G. J. Kleywegt and T. A. Jones, *ESF/CCP4 Newsletter No. 28* (1993), p. 56.
23. K. Cowtan, *ESF/CCP4 Newsletter No. 31* (1994), p. 34.
24. T. A. Jones, *J. Appl. Crystallogr.* **11**, 268 (1978).
25. T. E. Ferrin, C. C. Huang, L. E. Jarvis, R. Langridge, *J. Mol. Graphics* **6**, 13 (1988).
26. R. Esnouf, personal communication.
27. P. J. Kraulis, *J. Appl. Crystallogr.* **24**, 946 (1991).
28. A. C. Wallace, R. A. Laskowski, J. M. Thornton, *Protein Eng.* **8**, 127 (1995).
29. We thank the support staff at the Synchrotron Radiation Source at Daresbury Laboratory for assistance with station alignment. Supported by grants from the UK Biotechnology and Biological Sciences Research Council (BBSRC) and Medical Research Council (D.W.R. and A.R.S.). C.B. is funded by a Zeneca Agrochemicals-supported CASE award. J.B.R. is a BBSRC David Phillips Research Fellow. The Krebs Institute is a designated BBSRC Biomolecular Science Centre.

2 August 1996; accepted 15 October 1996

Orientation Maps of Subjective Contours in Visual Cortex

Bhavin R. Sheth, Jitendra Sharma, S. Chenchal Rao, Mriganka Sur*

Responses to subjective contours in visual cortical areas V1 and V2 in adult cats were investigated by optical imaging of intrinsic signals and single-unit recording. Both V1 and V2 contain maps of the orientation of subjective gratings that have their basis in specific kinds of neuronal responses to subjective orientations. A greater proportion of neurons in V2 than in V1 show a robust response to subjective edges. Through the use of subjective stimuli in which the orientation of the luminance component is invariant, an unmasked V1 response to subjective edges alone can be demonstrated. The data indicate that the processing of subjective contours begins as early as V1 and continues progressively in higher cortical areas.

Contours that are perceived under stimulus configurations in which the stimulus lacks any physical discontinuity (such as a luminance border) are termed subjective or illusory contours. Subjective contours and subjective shapes can be perceived in a manner analogous to the perception of luminance

contours and shapes (1), suggesting that subjective and luminance contours might be processed in similar manner, perhaps by similar neural substrates. A subset of neurons in V2 of monkeys has been shown to respond to subjective edges (2). In addition, cells in monkey V1 have been reported to respond to subjective edges (3); however, the stimuli used were different from classical subjective stimuli because they had a luminance gradient across the putative "subjective" edge. Thus, the question of whether or not V1 neurons respond to subjective stimuli remains unresolved. Further-

Department of Brain and Cognitive Sciences, Massachusetts Institute of Technology (MIT), Cambridge, MA 02139, USA.

*To whom correspondence should be addressed at Department of Brain and Cognitive Sciences, MIT, E25-235 Cambridge, MA 02139, USA. E-mail: msur@wccf.mit.edu

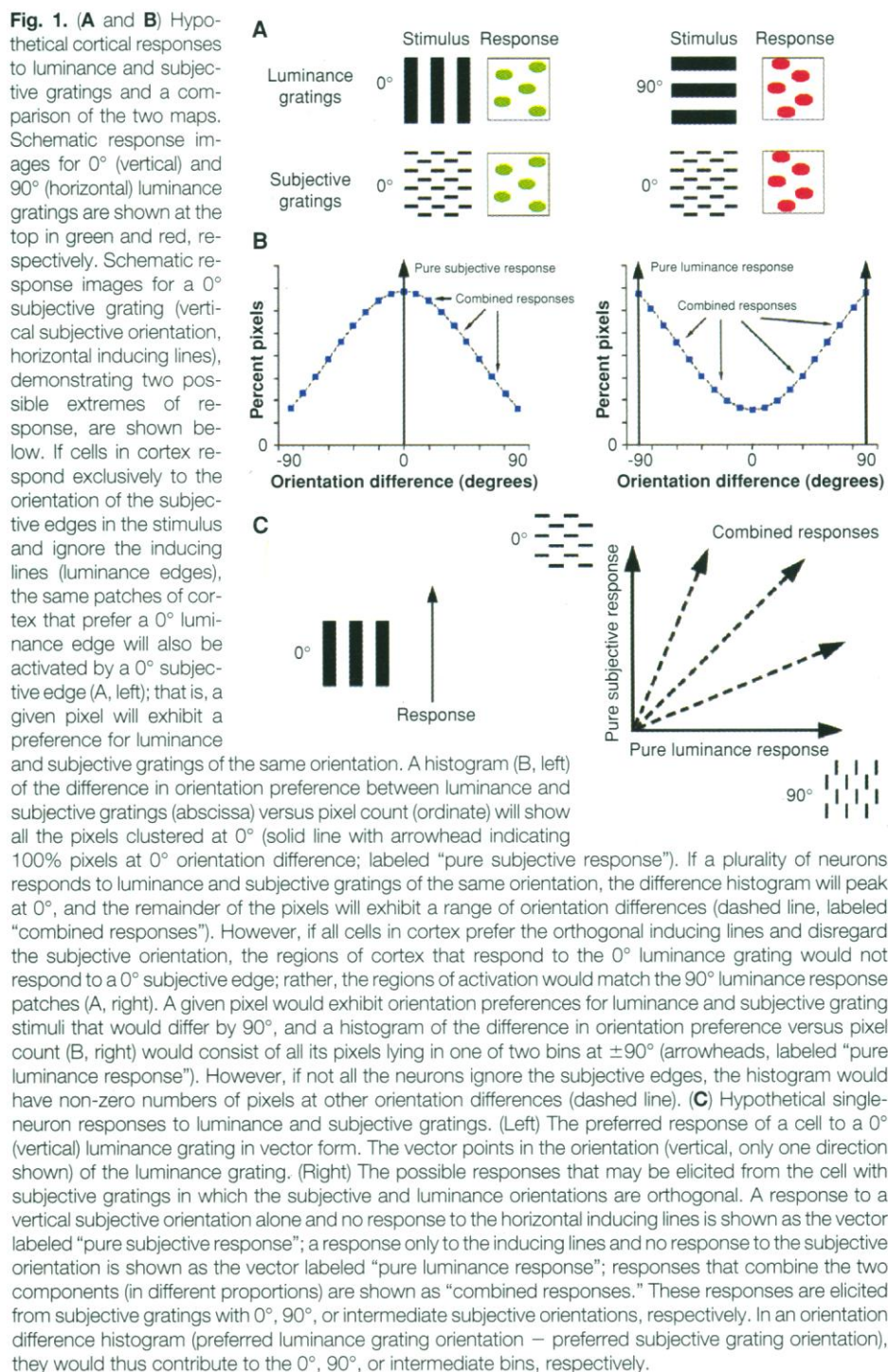
more, whether cells responsive to subjective edges are organized into maps, and how the organization relates to that of cells responsive to luminance edges, remains open. We now demonstrate that cells in both V2 and V1 of cats are responsive to subjective edges, and cells with the same subjective orientation preference are clustered to form maps that bear a systematic relation to maps of orientation preference for luminance edges.

Cats perceive subjective contours (4) and are able to discriminate fine differences in the orientation of subjective edges (5). We investigated the ability of subjective contours to drive cells in V1 (area 17) and V2 (area 18) of adult cat visual cortex (6) using intrinsic signal optical imaging (7) and single-unit recording. To quantitatively compare cortical responses to subjective and luminance stimuli, we used luminance gratings composed of light and dark bars (or thinner lines), and subjective gratings composed of orthogonal inducing lines (Fig. 1A). If neurons in visual cortex signal the subjective orientation and ignore the orthogonal inducing lines (luminance edges), the locations of orientation domains imaged with luminance and subjective gratings should match closely (Fig. 1A, left). Thus, for each pixel comprising the optical map, the orientation preference for subjective and luminance gratings should be nearly identical. A histogram of pixel count showing the difference in orientation preference obtained with the two types of stimuli should therefore yield a histogram with all of the pixels comprising the bin at 0° orientation difference (Fig. 1B, left). Conversely, if neurons respond solely to the inducing lines and ignore the orthogonal subjective edges (Fig. 1A, right), maps for luminance and subjective gratings should be complementary (compare, for example, the hypothetical maps at upper left and lower right of Fig. 1A). A histogram of pixels showing the difference in orientation preference between the two maps would therefore show all pixels in the bins at $\pm 90^\circ$ orientation difference (Fig. 1B, right). In either instance, pixels at an orientation difference intermediate between 0° and $\pm 90^\circ$ would represent combined responses to both subjective and luminance components of the subjective grating (Fig. 1B). The single-neuron responses that underlie such optically imaged maps are shown in Fig. 1C. The tuned response of a cell to a luminance grating is shown in vector form in Fig. 1C (left), whereas possible responses to subjective gratings with orthogonal subjective and luminance orientations are shown in Fig. 1C (right). A cell could respond to the subjective component alone (Fig. 1C, right, "pure subjective response"), to the inducing

lines alone (Fig. 1C, right, "pure luminance response"), or to a combination of the two (Fig. 1C, right, "combined responses"). These response types would be represented in the orientation difference histograms of Fig. 1B as lying, respectively, in the 0°, $\pm 90^\circ$, or intermediate orientation difference bins.

Responses from a patch of V2 (8) to gratings of similar luminance and subjective orientations are shown in Fig. 2, A and B, respectively. Their orientation domains

overlap in spatial location and extent. The composite luminance and subjective grating maps (9), combining the responses at all stimulus orientations (10), are shown in Fig. 2, C and D. We determined the relative contributions of the subjective and luminance components of the subjective grating to the cortical response by computing the difference in orientation preference between luminance and subjective gratings for each pixel (a map of "subjective signal strength") (11). The resultant difference

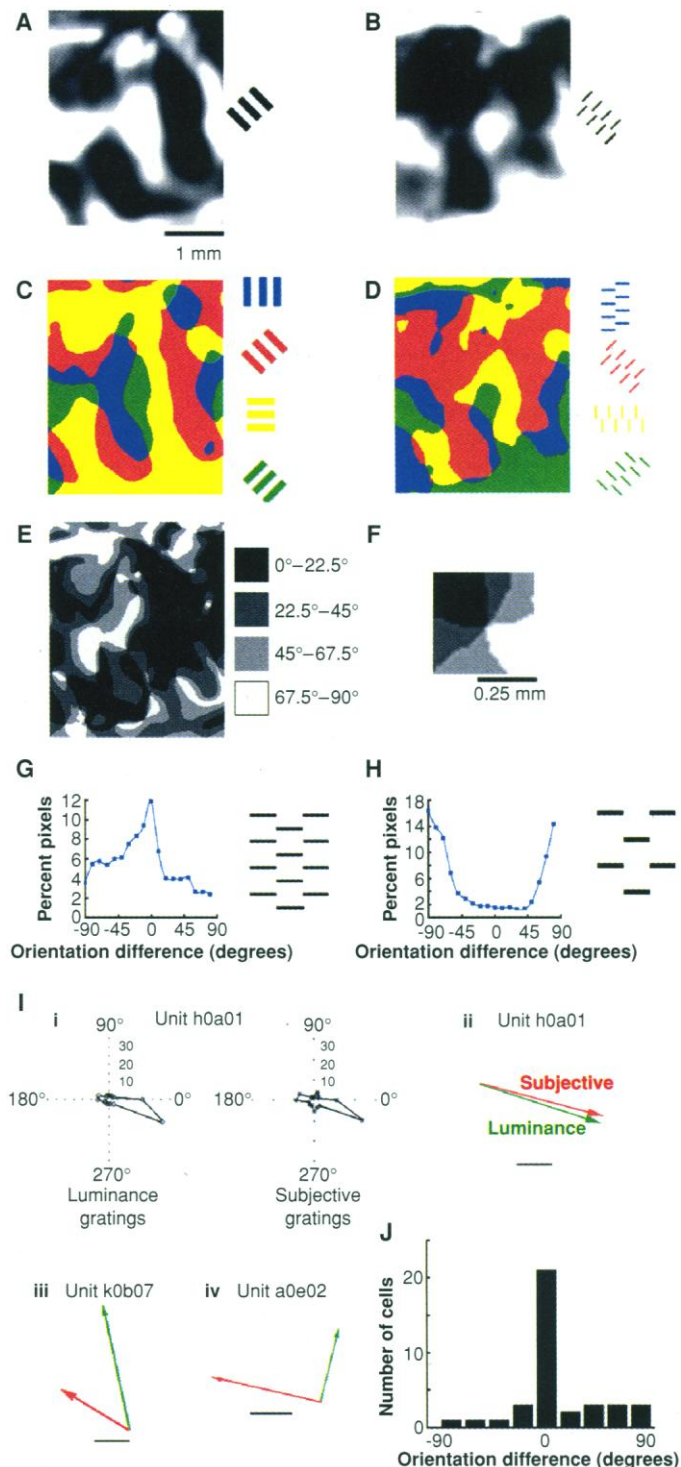


map is shown in Fig. 2E (regions with an orientation difference less than $\pm 22.5^\circ$ are shown in black, regions with an orientation difference greater than $\pm 67.5^\circ$ are shown in white). The orientation difference map shows that a substantial portion of V2 (coded in black) has a preference for similar

luminance and subjective orientations. The map also demonstrates that the orientation preference of neurons for the luminance and subjective components of subjective gratings varies smoothly across the cortical surface (darker shades of gray represent progressively stronger preference for the sub-

jective edges relative to the inducing lines). Neurons with a given response preference are clustered, and neurons with adjacent preferences are organized, in specific places, in a radial, pinwheel-like manner (Fig. 2F shows a typical radial organization at a higher magnification). The density of pin-

Fig. 2. Optical and single-unit responses to subjective gratings in V2. **(A and B)** Differential maps for (A) luminance gratings and (B) subjective gratings. The differential maps were obtained by subtracting the raw images in response to a 135° grating, summed and averaged over all stimulus trials, from the raw images in response to a 45° grating for the same set of trials (see text for details). The spatial frequency of luminance and subjective gratings (subjective edges) was 0.15 cycle per degree each; the inducing lines were spaced at a frequency of 0.45 cycle per degree. **(C and D)** Composite orientation-preference maps in V2 for (C) luminance and (D) subjective gratings. To obtain these composite maps, we summed vectorially the response at each pixel to the stimulus orientations (including both directions of motion) and displayed the resultant angle of preferred orientation in pseudo-color according to the key at right. Luminance and subjective gratings of identical orientation are coded in the same color (for example, pixels that respond best to a vertical subjective grating and a vertical luminance grating are both shown in blue). **(E)** The map of orientation differences [comparing (C) and (D)]. For each pixel, the difference between its luminance and subjective orientation preference was computed and coded in one of four shades of gray: 0° to $\pm 22.5^\circ$, black; $\pm 22.5^\circ$ to $\pm 45^\circ$, dark gray; $\pm 45^\circ$ to $\pm 67.5^\circ$, light gray; and $\pm 67.5^\circ$ to $\pm 90^\circ$, white. **(F)** Magnified portion from (E), showing the pinwheel-like radial arrangement of neurons. Regions of positive and negative orientation difference are coded by the same gray level; hence each gray level is represented twice around a pinwheel center. **(G)** The pixel difference histogram comparing orientation preference for luminance and subjective gratings, derived from the maps in (C) and (D). The histogram shows a peak close to 0° orientation difference, indicating a strong response in V2 to subjective orientations. Twenty-two percent of pixels fell in the central 20° (-10° to $+10^\circ$) orientation difference, and 84% were within $\pm 70^\circ$ orientation difference. **(H)** Effect of inducing line density on subjective orientation responses in V2. Inducing line spatial frequency, 0.225 cycle/degree; only 3% of pixels fell in the central 20° (-10° to $+10^\circ$) orientation difference, and 46% were within $\pm 70^\circ$ orientation difference. The histograms in (G) and (H) were significantly different ($P < 0.001$, χ^2 test). **(I)** Examples of single-neuron responses to subjective gratings in V2. (i) Polar plots of responses to drifting luminance and subjective gratings from a complex, non-end-stopped cell in V2. The angle of stimulus motion is plotted along the circle, and the magnitude of the cell's response (in spikes per second) is plotted radially. The cell had a receptive field of dimensions 12° by 10° , located at an eccentricity of 9° below the horizontal meridian. The cell responded best to an obliquely oriented luminance grating (i, left) moving down and to the right, and to a subjective grating (i, right) of the same orientation and direction. (ii) The responses to luminance or subjective gratings of eight different orientations were summed vectorially, in the same manner as for each pixel in the imaging experiments. The resultant orientation vector shows the cell's luminance (shown in green) and subjective (shown in red) orientation preferences and the magnitude of its response to the preferred orientations (represented by vector length). These are orientation vectors, with angles that vary between 0° and 180° . The preferred luminance and subjective orientations of the cell were nearly identical (differing by 3°), indicating a response to the subjective orientation alone. Bar, 10 spikes per second. (iii) A cell whose luminance and subjective orientation preferences differed by 47° , indicating a nearly equal combination of responses to the subjective and luminance components of the subjective grating. Bar, 1 spike per second. (iv) A cell whose luminance and subjective orientation preferences were nearly orthogonal (differing by 89°), indicating a response solely to the luminance-defined inducing lines. Bar, 5 spikes per second. **(J)** Frequency histogram of the difference in orientation preference between luminance and subjective gratings of V2 neurons ($n = 38$). Each cell's luminance and subjective orientation preferences were obtained as above. Cells were then binned into 20° bins depending on the difference between the two; neurons whose orientation preference for luminance and subjective gratings differed by a value within -10° to $+10^\circ$ were summed into the central bin (21 cells, 55%), and so on. In addition, 7 cells did not show a clear orientation preference for luminance gratings and 12 cells did not respond to either the subjective edges or the inducing lines.



wheels is 2.3 per square millimeter. The difference histogram (Fig. 2G), quantifying the difference map of Fig. 2E, shows that a large proportion of pixels respond to similarly oriented luminance and subjective gratings. These results, which are representative of maps from V2 in three animals, demonstrate that many neurons in V2 respond in an orientation-specific manner to subjective gratings, and that these neurons are organized into maps of orientation preference that bear a systematic relation to those for luminance gratings.

The spacing between inducing lines is important in the perception of subjective contours (5). We doubled the spacing between the inducing lines (and also doubled the thickness of each individual line in order to maintain the same overall stimulus luminance) and observed a marked change in the V2 response. The same cortex that showed a clear response to subjective edges composed of a high density of inducing lines (Fig. 2G) now gave a strong response to the inducing lines with little or no response to the subjective edges in the stimulus (Fig. 2H). Thus, changing the density of inducing lines changes the physiological response of V2 to subjective gratings.

Single-unit recordings in V2 (12), in which the same stimuli were used as for optical imaging, showed that individual neuron responses were consistent with the imaging results. A V2 cell that responded best to the same orientation of luminance and subjective gratings is shown in Fig. 2I (i and ii). Apart from such neurons that respond to subjective edges alone, V2 also contains neurons that respond to a combination of subjective edges and inducing lines [Fig. 2I (iii)] or to the inducing lines alone [Fig. 2I (iv)] in the subjective grating. Of all cells recorded in V2 that responded to subjective gratings (38 of 57 cells), 21 cells showed a response to subjective gratings with a preferred orientation within $\pm 10^\circ$ of the preferred orientation of luminance gratings (Fig. 2J), indicating that these cells responded almost exclusively to the subjective edges in the subjective grating. For another 13 cells, responses to subjective gratings were tuned to an orientation intermediate between $\pm 10^\circ$ and $\pm 70^\circ$ of their preferred luminance grating orientation, indicating that these cells carried signatures of both luminance and subjective components in their responses (13). Together, the majority of V2 neurons in our sample (60% of cells) conveyed information about subjective orientations (14).

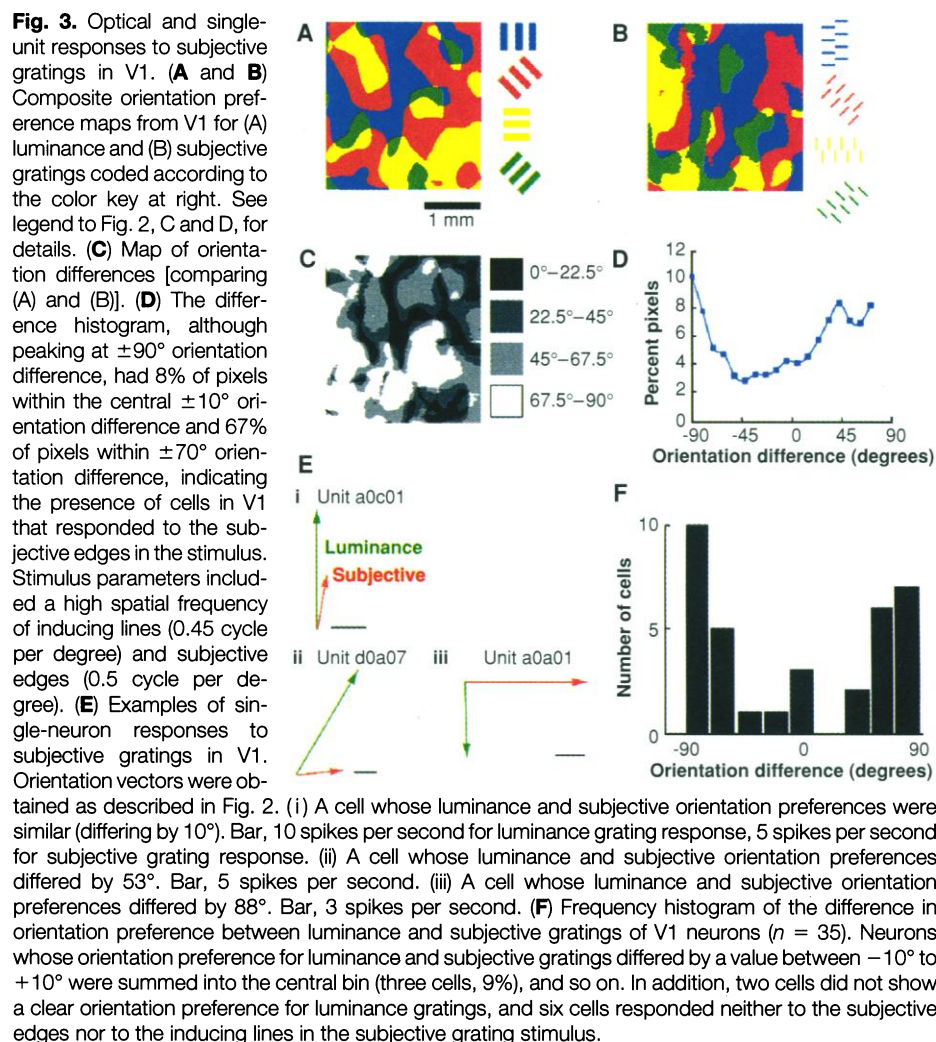
We next examined V1 responses to subjective gratings constructed with stimulus parameters derived from the known stimulus selectivity of V1 cells (15) (four animals). Maps of V1 in response to luminance grat-

ings and to subjective gratings with a high spatial frequency of inducing lines are shown in Fig. 3, A and B, respectively. The orientation difference map showed the presence of regions (Fig. 3C, coded in shades of gray) whose response depended to a varying extent on the orientation of subjective edges. In specific regions of the map, these cells were also organized in a pinwheel-like manner. Although the orientation difference maps in V1 and V2 demonstrated that fewer pixels in V1 than in V2 prefer the same luminance and subjective orientation (compare Figs. 3C and 2E), the orientation preference for luminance and subjective components varied smoothly across the V1 map as well. The density of pinwheels in V1 (2.8 per square millimeter) was comparable to that in V2. The difference histogram quantifying Fig. 3C peaked at $\pm 90^\circ$ orientation difference but had other local maxima, some fraction of pixels at 0° orientation difference, and a high fraction of pixels with intermediate orientation differences (see legend to Fig. 3D). Thus, a demonstrable proportion of cells in V1 respond to subjective edges alone or in

combination with luminance edges in the subjective grating (16).

Single cells in V1, as in V2, showed a range of responses to subjective gratings, although the proportion of cells with the various types of response was different in the two cortical areas. Figure 3E shows cells in V1 that responded almost exclusively to the orientation of subjective edges (i), to a combination of both luminance and subjective edges in the subjective grating (ii), or to the inducing lines alone (iii). Of the cells in V1 that responded to subjective gratings (35 of 43 cells), 3 had a preference for subjective grating orientation that was less than $\pm 10^\circ$ offset from the cell's preferred luminance grating orientation, and 15 others showed a preference for intermediate orientations. Thus, the single-cell data confirm that a reasonable proportion of cells in V1 (42% in our sample) respond to either the subjective component alone or in combination with the luminance component of the subjective grating (17, 18).

To further examine the responses of V1 neurons to subjective edges, we devised stimuli to differentiate as unambiguously as pos-



sible between cortical responses attributable to the subjective and luminance parts of the stimulus. We imaged the response of visual cortex to a pair of stimuli that had identical inducing line orientation, identical direction of motion (orthogonal to the inducing lines), and that differed in a single stimulus parameter—the orientation of the subjective edge (Fig. 4A). We found distinct dark and light patches in V2 and V1 (19) corresponding to orientation domains for the two orthogonal subjective orientations. If the cortex did not contain columns segregated for subjective orientation preference, subtracting the response to one subjective stimulus orientation from that to the orthogonal orientation would result in a homogeneous optical map (the orientation signal from the inducing lines is the same for both stimuli, and subtraction of the two optical images will eliminate the common luminance signal). However, the resultant map consists of response clusters that are elicited by the subjective orientations (Fig. 4A). The orientation-specific response of a cell in V1 to the luminance-invariant subjective grating is shown in Fig. 4B. A majority of cells (11 of 13 cells) recorded in V1 showed an unequivocal response to a particular subjective orientation (Fig. 4C); 8 of these cells responded well to the inducing lines in the conventional subjective grating stimulus (with orthogonal inducing lines). Thus, the subjective response component of V1 cells appears to be unmasked when examined with subjective grating stimuli in which the orientation of the luminance component is invariant. When subjective gratings with orthogo-

nal inducing lines are used, the important difference between V1 and V2 might be not whether V1 cells have a subjective component to their responses, but rather the extent to which a luminance component is expressed in, and masks, responses of V1 cells to subjective edges.

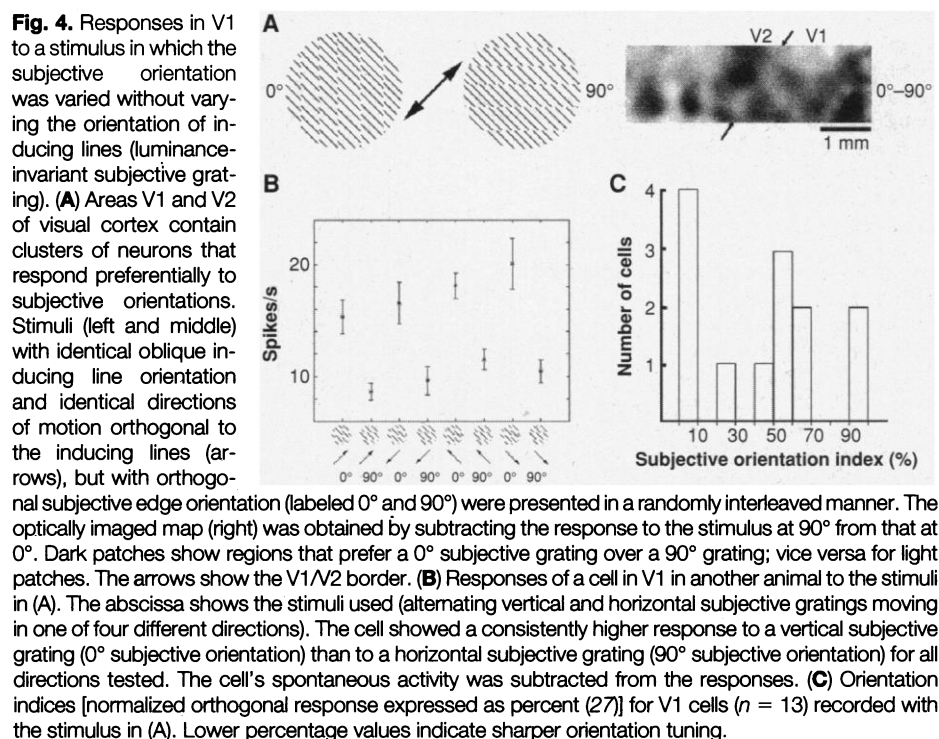
Cells in both areas V1 and V2 of cats are orientation-selective and cluster to form columns whose cells share the same orientation preference for luminance edges (20, 21) (Figs. 2C and 3A). We have confirmed that V2 contains neurons that respond to the orientation of subjective edges (2, 22), and we now show that (i) V1 also contains neurons that respond to the same kind of subjective stimuli, and (ii) in both areas, these neurons are clustered in discrete columns and organized into maps of subjective orientation preference. The maps show, in places, a radial, pinwheel-like arrangement of orientation differences (between preferred subjective and luminance orientations). A sizable number of cells in both V1 and V2 respond to at least a combination of subjective and luminance edges in the subjective grating. Specifically, V1 and V2 contain cells that respond almost exclusively to the subjective edges, the inducing lines alone, or a combination of the two. However, the relative proportions of these cells differ between the two areas: a greater proportion of cells in V2 than in V1 show a nearly exclusive response to subjective edges. At the same time, the majority of V1 cells can potentially convey information about subjective orientations, as revealed through the use of a luminance-

invariant subjective stimulus. Subjective orientations appear to be signaled in a distributed manner, through the activity of large numbers of neurons in V1 and V2.

Our study shows that even a complex visual attribute, such as subjective contour orientation, can be extracted and systematically represented in the earliest stage of visual cortex, V1 (23). The processing of subjective contours continues to the next cortical stage, V2 (24), with more neurons providing the perceptual signals related to a subjective orientation. The presence of neurons responsive to subjective edges in V1 and V2, their clustering into modules, and their organization into maps argues for an intricate level of network organization that far exceeds the complexity associated with these areas so far (25).

REFERENCES AND NOTES

1. L. Schumann, *Z. Psychol.* **23**, 1 (1900); G. Kanizsa, *Riv. Psychol.* **49**, 7 (1955); *Organization in Vision: Essays on Gestalt Perception*, G. Kanizsa, Ed. (Praeger, New York, 1979), p. 192; J. J. Koenderink, *Perception* **13**, 321 (1984).
2. R. von der Heydt, E. Peterhans, G. Baumgartner, *Science* **224**, 1260 (1984); R. von der Heydt and E. Peterhans, *J. Neurosci.* **9**, 1731 (1989).
3. D. H. Grosz, R. M. Shapley, M. J. Hawken, *Nature* **365**, 550 (1993).
4. M. Bravo, R. Blake, S. Morrison, *Vision Res.* **28**, 861 (1988).
5. P. De Weerd, P. E. Vandenbussche, B. De Bruyn, G. A. Orban, *Behav. Brain Res.* **39**, 1 (1990).
6. Adult cats ($n = 18$) were used in these experiments. All experiments were performed under protocols approved by MIT's Animal Care and Use Committee. Anesthesia was induced with ketamine [15 mg per kilogram of body weight, intramuscular (im)] and xylazine (1.5 mg/kg, im) and maintained with isoflurane (typically 0.5 to 1.5% in 70/30 N₂O/O₂) delivered through a tracheal cannula. Cats were paralyzed with an intravenous combination of gallamine triethiodide (3.6 mg/hour) and tubocurarine chloride (0.15 mg/hour) and artificially respired to maintain end-tidal CO₂ volume at ~4% at a partial pressure of 30 ± 3 mm Hg. The animal's electroencephalogram and heart rate were monitored continuously to ensure adequate anesthesia. Craniotomy followed by durotomy was performed to expose visual cortex. For imaging area V2, we centered our chamber at A4 and recorded from an area that extended approximately from A3 to A7 in the anteroposterior direction and between L0.5 to L3.5 in the mediolateral direction. For imaging V1, the chamber was centered at P5 and a similar expanse of cortex was exposed. For imaging V1 and V2 simultaneously, the chamber was centered at A0 [R. J. Tusa, L. A. Palmer, A. C. Rosenquist, *J. Comp. Neurol.* **177**, 213 (1978); R. J. Tusa, A. C. Rosenquist, L. A. Palmer, *ibid.* **185**, 657 (1979)].
7. Techniques for intrinsic signal imaging were similar to those described by Grinvald *et al.* [A. Grinvald, E. Lieke, R. D. Frostig, C. D. Gilbert, T. N. Wiesel, *Nature* **324**, 351 (1986)] and used by us previously (26). A stainless-steel recording chamber was attached to the skull surrounding the craniotomy, filled with silicone oil, and then sealed with a quartz plate. A video camera (CCD-5024N Bishke, Japan, RS-170, >60 dB signal to noise ratio) consisting of a 655 by 480 array of pixels equipped with a tandem-lens microscope [E. H. Ratzlaff and A. Grinvald, *J. Neurosci. Methods* **36**, 127 (1991)] was positioned over the cortex. This arrangement gave a magnification of 75 pixels per millimeter. Data were collected by means of an imaging system (Optical Imaging). The camera signal was amplified by a video enhancement amplifier; a baseline image was subtracted from each stimulus response image in analog form and then



digitized by an 8-bit analog-to-digital converter (Matrox) installed on a 486-66 PC. Initially, a reference map of the blood vessel pattern at the surface of the cortex was obtained by means of light filtered at 550 ± 40 nm (Ealing). The camera was then focused 300 μ m below the surface of the cortex. Light from a 100-W tungsten-halogen light source driven by a dc power supply (Kepeco) was passed through a 610-nm filter and used to illuminate the cortex during data collection. Frames were summed between 0.9 to 3.6 s after stimulus onset, corresponding to the time of maximum signal as determined by our previous experiments (26). Data were analyzed with the use of in-house programs written in C++ (Borland) and IDL Research Systems.

8. Square-wave luminance gratings (typical parameters for V2: spatial frequency, 0.15 cycle per degree; drift velocity, 12° per second; 64% contrast) and subjective gratings (typical spatial frequency of subjective orientation, 0.15 cycle per degree; spatial frequency of inducing lines, 0.45 cycle per degree; drift velocity, 12° per second for V2) were shown to the animal on a 17-inch monitor positioned 28.5 cm in front of it. In some experiments, the spatial frequency of subjective edges was systematically varied. Neutral gray intensity was 6.0 cd/m². All stimuli were shown binocularly. Subjective grating stimuli of four different orientations (0°, 45°, 90°, and 135°) were randomly interleaved with square-wave luminance grating stimuli and presented 80 to 100 times. Luminance-defined inducing lines, 1 to 2 pixels wide, were orthogonal to the subjective orientation for all subjective grating stimuli. Gratings were drifted normal to the subjective edge orientation and parallel to the orientation of the inducing lines in both directions separately. Eye position and area central of both eyes were checked at the start of imaging by use of a reverse ophthalmoscope to project an image of the retinal vasculature onto the screen.
9. Orientation maps obtained with luminance gratings composed of thin lines (of the same width as the subjective grating inducing lines) were identical to orientation maps obtained with thicker bars (Fig. 2C) and relatively independent of grating spatial frequency.
10. We compared orientation strengths (magnitude of the orientation vector) for those pixels in V2 (Fig. 2, C and D) that had similar orientation preferences for luminance and subjective gratings (within $\pm 22.5^\circ$ orientation difference). The mean orientation strength for luminance gratings (4.56×10^{-3} units) was threefold higher than the mean orientation strength for subjective gratings (1.31×10^{-3} units) for these pixels.
11. We vectorially summed the responses of each pixel to all orientations of luminance and subjective gratings separately, obtained the pixel's resultant orientation preferences for both, and derived the difference between the two values.
12. Single-unit experiments were carried out in 12 cats. Single units were recorded with parylene-insulated tungsten microelectrodes. Responses were conventionally amplified, displayed, and stored. Stimulus conditions were the same as in the imaging studies.
13. Receptive field properties of a subset of V2 cells whose luminance and subjective orientation preferences differed by $\pm 45^\circ$ or less (17 cells) were studied in detail. Most of these cells (13 cells) were complex; four cells were simple. Only 2 of the cells were end-stopped; the remainder (15 cells) were non-end-stopped. Twenty-four cells whose locations were identified were encountered at a variety of depths (160 to 1800 μ m); 11 cells were encountered in the superficial layers and 13 cells in the deep layers.
14. We correlated the responses of single neurons ($n = 7$) to luminance and subjective gratings with the optically imaged maps. Each of the regions in the orientation difference map—in which orientation preferences for luminance and subjective orientations are similar, orthogonal, or in-between—contained neurons with matching responses.
15. J. A. Movshon, I. D. Thompson, D. J. Tolhurst, *J. Physiol.* **283**, 101 (1978); K. Albus, *Exp. Brain Res.* **24**, 159 (1975).
16. We compared orientation strengths for those pixels in V1 (Fig. 3C) that had similar orientation preferences for luminance and subjective gratings (within

$\pm 22.5^\circ$ orientation difference). The mean orientation strength for subjective gratings (1.00×10^{-3} units) was slightly higher than the mean orientation strength for luminance gratings (0.87×10^{-3} units) for these pixels. Thus, the response to subjective gratings in V1 was stronger for subjective gratings than for luminance gratings for this subset of pixels, although they occupied a small portion of V1.

17. Receptive field properties of a subset of V1 cells whose luminance and subjective orientation preferences differed by $\pm 45^\circ$ or less were studied in detail. Three cells were complex; one was a simple cell. Two cells were end-stopped, four cells were non-end-stopped. Six cells whose locations were identified were encountered at depths ranging from 300 to 1200 μ m from the surface.
18. Responses to subjective gratings cannot be explained by responses to line terminations. We have shown that cells that share the same orientation preference for luminance and subjective gratings may respond optimally to a grating composed of a grid of dots (line ends) with the same parameters (spatial frequency, temporal frequency) as the subjective grating but of an entirely different orientation. Some cells that are tuned to the same orientation of luminance and subjective gratings as well as the dot grid show a sharper tuning, or a higher response, or both, to a subjective grating than to a dot grid. A response to Fourier energy alone cannot explain why the response of a cell to an intermediate subjective orientation is higher than the response at 90° orientation difference (orientation of the inducing lines in the subjective grating), because the energy along these orientations is less than the energy along the inducing-line orientation. Moreover, most such cells respond optimally to a single intermediate orientation, despite the presence of equal Fourier energy in the stimulus along both the optimal orientation and its orthogonally oriented counterpart.
19. V2 and V1 in cats are anatomically distinct [R. Otsuka and R. Hassler, *Arch. Psychiatr. Nervenkr.* **203**, 212 (1962); D. J. Price, *Exp. Brain Res.* **58**, 125 (1985); G. H. Kageyama and M. Wong-Riley, *J. Comp. Neurol.* **243**, 182 (1986); B. R. Payne, *Vis. Neurosci.* **6**, 445 (1990); A. L. Humphrey, M. Sur, D. J. Uhlich, S. M. Sherman, *J. Comp. Neurol.* **233**, 190 (1985)]. To physiologically assess the boundary between V1 and V2, we used luminance gratings with different param-

eters: a grating of high spatial frequency (0.5 cycle per degree) and low drift velocity (4° per second), which V1 neurons prefer, and a grating of low spatial frequency (0.15 cycle per degree) and high drift velocity (12° per second), which V2 neurons prefer [(21)]. By distinguishing the portion of the optically imaged region that responded preferentially to the slower drift rate, higher spatial frequency stimulus (V1) compared to the higher drift rate, lower spatial frequency stimulus (V2), we could locate the V1/V2 boundary accurately. The physiological border coincided with the anatomical border between areas 17 and 18 as demonstrated by marker lesions and histology.

20. D. H. Hubel and T. N. Wiesel, *J. Physiol. (London)* **165**, 559 (1963); *ibid.* **195**, 215 (1968); T. Bonhoeffer and A. Grinvald, *J. Neurosci.* **13**, 4157 (1993).
21. T. Bonhoeffer, D.-S. Kim, D. Maloney, D. Shoham, A. Grinvald, *Eur. J. Neurosci.* **7**, 1973 (1995).
22. C. Redies, J. M. Crook, O. D. Creutzfeldt, *Exp. Brain Res.* **61**, 469 (1986).
23. See also A. F. Rossi, C. D. Rittenhouse, M. A. Paradiso, *Science* **273**, 1104 (1996); V. A. Lamme, *J. Neurosci.* **15**, 1605 (1995); D. A. Leopold and N. K. Logothetis, *Nature* **379**, 549 (1996).
24. V1 and V2 in cats differ in their thalamic inputs as well: V1 receives input from X and Y cells located in the A-laminae of the lateral geniculate nucleus, whereas V2 receives inputs from Y cells alone [reviewed in S. M. Sherman and P. D. Spear, *Physiol. Rev.* **62**, 738 (1982)].
25. R. L. Gregory, *Nature* **238**, 51 (1972); *ibid.* **199**, 678 (1963); I. Rock and R. Anson, *Perception* **8**, 665 (1979).
26. S. C. Rao, L. J. Toth, B. R. Sheth, M. Sur, *Soc. Neurosci. Abstr.* **20**, 836 (1994); L. J. Toth, S. C. Rao, D.-S. Kim, D. Somers, M. Sur, *Proc. Natl. Acad. Sci. U.S.A.* **93**, 9869 (1996).
27. S. Nelson, L. J. Toth, B. Sheth, M. Sur *Science* **265**, 774 (1994).
28. We thank D.-S. Kim and L. Toth for assistance and E. Adelson, B. Anderson, and P. Sinha for critical reading of the manuscript. Supported by NIH grant EY07023. J.S. was supported by a fellowship from the Fogarty International Center of the NIH.

18 September 1996; accepted 28 October 1996

Requirement of CDC42 for *Salmonella*-Induced Cytoskeletal and Nuclear Responses

Li-Mei Chen, Silke Hobbie, Jorge E. Galán*

The bacterial pathogen *Salmonella typhimurium* triggers host cell signaling pathways that lead to cytoskeletal and nuclear responses required for pathogenesis. Here, the role of the small guanosine triphosphate (GTP)-binding protein CDC42Hs in these responses was examined. Expression of a dominant interfering mutant of CDC42 (CDC42HsN17) prevented *S. typhimurium*-induced cytoskeletal reorganization and subsequent macropinocytosis and bacterial internalization into host cells. Cells expressing constitutively active CDC42 (CDC42HsV12) internalized an *S. typhimurium* mutant unable to trigger host cell responses. Furthermore, expression of CDC42HsN17 prevented *S. typhimurium*-induced JNK kinase activation. These results indicate that CDC42 is required for bacterial invasion and induction of nuclear responses in host cells.

Interaction of the bacterial pathogen *Salmonella typhimurium* with host cells activates a bacterially encoded protein secre-

tion system that directs the export and, in some cases, the translocation into the host cell of several bacterial proteins (1). These proteins, in turn, trigger signal transduction pathways that lead to a variety of cellular responses.

Among these responses is an extensive reorganization of the actin cytoskeleton, re-

Department of Molecular Genetics and Microbiology, School of Medicine, State University of New York at Stony Brook, Stony Brook, NY, 11794-5222, USA.

*To whom correspondence should be addressed.